doi:10.1088/1742-6596/2647/11/112009

# Stochastic flutter analysis of a torsional-vibrationbased energy harvester affected by random aeroelastic loads and wind turbulence

# Davide Piciucco and Luca Caracoglia

Department of Civil and Environmental Engineering, Northeastern University, 360 Huntington Avenue, Boston, MA 02115, USA

E-mail: davide.piciucco@hotmail.com, lucac@coe.neu.edu

Abstract. This paper investigates the energy production of a "meso-scale", wind-based energy harvester that exploits the torsional aeroelastic instability of a rigid blade-airfoil, elastically supported at equidistant supports. Torsional flutter is a single mode aeroelastic instability phenomenon, in which a diverging dynamic angular rotation of a body occurs. The apparatus relies on a simple mechanism that uses flow-induced pitch motion to extract and convert airflow kinetic energy to electrical energy. The system is composed by a rigid blade-airfoil, connected to a support structure through a non-linear restoring force (torsional spring-like) mechanism that enables the rotation about a reference pivot axis. The proposed technology is designed to be efficient in the range of low and medium wind speeds (10-13 m/s), in which horizontal-axis wind turbines and other harvesters are not efficient. Deterministic pre-flutter, incipient flutter and post-critical vibrations of the apparatus have been already explored in a previous study. This work aims to further investigate the aeroelastic behavior of the "flapping foil" by examining the effect of turbulence, random experimental error and modeling simplifications of the aeroelastic forces. The analysis is conducted at incipient flutter in the frequency domain using classical unsteady force models. Monte Carlo methods are employed to solve for the probability of incipient flutter speed. Several configurations are considered to improve the efficiency of the energy harvester.

#### 1. Introduction

The recent increasing demand for electricity and renewable energy has encouraged the use of innovative wind-based methods for power extraction. Both macro-scale systems (scale of several hundred meters), i.e., large onshore and offshore wind turbines, and micro-scale energy harvesters (scale of few centimeters for self-recharging sensors) have been investigated in the literature [1]. On the contrary, meso-scale devices at intermediate scales (few meters), are still a partially uncharted research and technology solution. This type of devices has promising potential for growth and innovation. To bridge this gap, a meso-scale system that exploits the torsional flutter to extract wind energy, has been proposed [2]. Torsional flutter is a single mode aeroelastic instability that often leads to catastrophic consequences in civil and aeronautical structures. The idea is to favorably exploit this phenomenon to extract and convert airflow kinetic energy to electrical energy. This concept originates from pioneering studies by Duncan [3] and McKinney and De Laurier [4], who first proposed torsional-flutter-based wind power generators ("flutter-mills"). This research field has received increasing attention in the last decades; a general

Content from this work may be used under the terms of the Creative Commons Attribution 4.0 licence. Any further distribution of this work must maintain attribution to the author(s) and the title of the work, journal citation and DOI.

doi:10.1088/1742-6596/2647/11/112009

overview of the available solutions is provided by Youn et al. [5]. FOr example, a simple Single-Degree-Of-Freedom (SDOF) power generator was proposed by Ahmadi [6, 7], who investigated the power production of an H-section with curved flanges undergoing flutter instability. He concluded that the simple SDOF device works at medium wind velocity, while its efficiency rapidly decreases with increasing wind speed because of a non-optimal choice of the cross sectional shape. Plate like flutter-mills were investigated by Tang et al. [8] and Matsumoto et al. [9, 10]. In particular, the former study examined the energy transfer between a cantilevered flexible plate and an axial fluid flow. The energy transmission is analyzed at various location of the plate and at different wind speeds. The study also demonstrated the efficiency of a compact thin plate flutter-mill.

In general, the extraction of power from the flow through a flapping foil relies on a mechanism that uses pitching and heaving motion. Several solutions have been proposed in the literature with fully prescribed motion [11], semi-passive motion (i.e., where either pitching or heaving is prescribed) [12, 13] or fully passive motion [14, 15]. Two-DOF flapping foils, elastically supported in heaving motion with mechanically driven pitching mode, have been investigated [13, 12]. Based on the same concept, Matsumoto [9] proposed a flutter power generator system composed by a 2DOF rectangular plate. He compared the efficiency of a forced heaving and a forced torsional oscillation system and concluded that the latter is more convenient as it stably generates wind energy at high wind speeds. The same concept was later expanded and examined experimentally by Pigolotti et al. [16].

More recently, Hoke et al. [17] numerically investigated the power performance of a 2DOF rectangular plate in a 2D constrained flow; a SDOF foil performing pitch oscillations has been tested by D'Adamo et al. [18], who demonstrated that the maximum propulsion force is obtained when the resonant wake frequency is tuned with the foil dynamics. New experimental tests performed on a 2DOF flapping foil were presented by Duarte et al. [19].

The solution proposed in this paper, designated as "leading-edge-flutter wind power generator" (LEFWPG), is similar to the system proposed by Ahmadi [6, 7] and consists in a SDOF (torsion only) "streamlined blade" with fully constrained heaving and passive pitch motion. The energy is produced exploiting an electro-magnetic induction conversion mechanism. The proposed technology is more competitive than existing, similar harvesters and traditional wind turbines since it works in the partially unexplored range of low and medium wind speeds (10 to 13 m/s). The proposed mechanism is also simpler than other 2DOF solutions as it relies on the pitch motion only (one DOF) and the streamlined cross section is less sensitive to undesirable aerodynamic effects than bluff sections [6]. The LEFWPG is also less impactful than large scale wind turbines and can be ideal for rooftop setting in small residential homes.

The technical feasibility of the proposed apparatus has been assessed in a previous study [2] as well as the deterministic pre-flutter, incipient flutter and post critical vibrations have been examined in [20]. This work investigates the effects of incoming flow turbulence and variability in the modelling of the aeroelastic moment on the critical reduced frequency and flutter wind speed.

In the second section of this paper, a general description of the apparatus and the pre-flutter and incipient flutter governing equations will be reported. In the third section the dynamic problem will be solved by introducing the random error in the aeroelastic force model, while the last section will be devoted to the analysis of turbulence effects on the critical flutter reduced frequency and velocity.

#### 2. Model description

#### 2.1. Conceptual design

The conceptual model of the apparatus is depicted in Fig. 1. Figure 1(a) presents a generic cross section in the horizontal plane (x, y), while the three-dimensional (3D) view of the system is

doi:10.1088/1742-6596/2647/11/112009

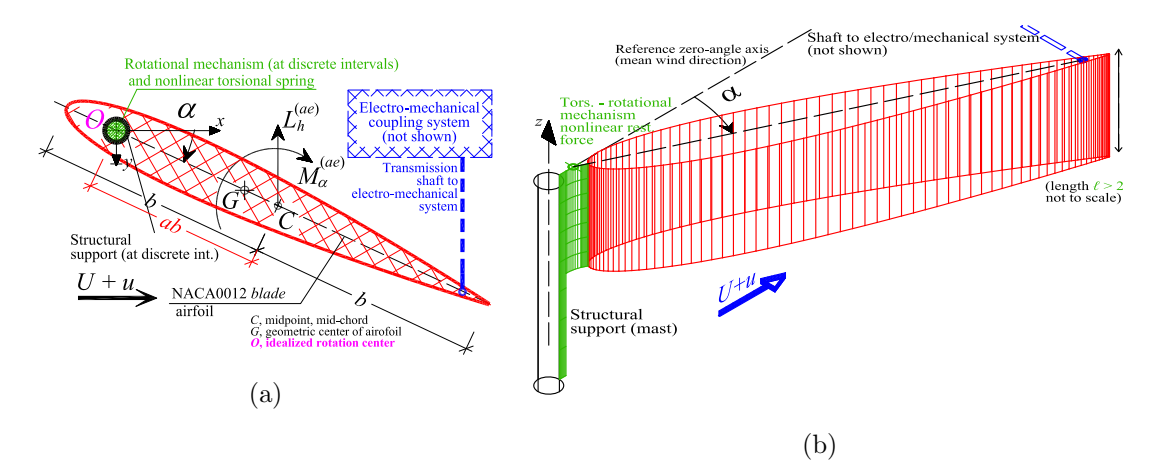


Figure 1: Conceptual model: (a) top view of a typical horizontal-plane cross-section, (b) 3D rendering of the apparatus with vertical-axis orientation and rotation axis at the leading edge (a = -1).

shown in 1(b). The model is composed of a rigid blade NACA0012 that rotates about a vertical axis (z) at pivot "O", at a distance ab from the mid-chord point (C). The variable a assumes negative values as long as the rotation axis is located on the wind-ward side, and a=-1 when the rotation axis is at the leading edge. The rigid blade has a chord length (width) 2b and transverse (longitudinal) length  $\ell$  in the z direction; the apparatus is vertically supported on a mast through a "torsional-rotational mechanism" to avoid dependence on gravity loads. The latter enables the rotation about the z axis ( $\alpha$  angle) about "O", by means of a non-linear torsional spring that controls the amplitude of the vibrations when instability occurs.

The energy conversion principle was inspired by an electromagnetic power generator [21]. The flapping blade is connected to a shaft equipped with a permanent magnet that translates through a coil, generating a magnetic field and electromotive forces. The coil is connected to an external circuit that induces current I(t) (t time).

# 2.2. Pre-flutter and incipient flutter problem

The equation of motion of the blade airfoil, neglecting electro-mechanical coupling effects, is:

$$\frac{\mathrm{d}^2 \alpha}{\mathrm{d}\tau^2} + 2\zeta_\alpha \frac{\mathrm{d}\alpha}{\mathrm{d}\tau} + \alpha = \frac{M_{oz}}{\omega_\alpha^2 I_{o\alpha}} \tag{1}$$

where  $\omega_{\alpha}$  is the angular frequency of the apparatus and  $\tau$  is a dimensionless time variable  $\tau = t\omega_{\alpha}$ . The structural damping is simulated through a linear term  $2I_{o\alpha}\zeta_{\alpha}$ ;  $I_{o\alpha}$  is the total polar mass moment of inertia. More information about electro-magnetic induced torque may be found in [20]. In the absence of turbulence, the unsteady torsional aeroelastic moment  $M_{oz}$  is derived from classical aerodynamic theory [22]:

$$M_{oz}(k) = \pi \rho \eta_{3D} b^2 U^2 \ell \int_0^\ell \left\{ -\alpha''(0.125 + a^2) + (2a+1)C(k,z)\alpha + + [(a-0.5) + (0.5 - 2a^2)C(k,z)]\alpha' \right\} dz$$
(2)

doi:10.1088/1742-6596/2647/11/112009

The mean aerodynamic forces are zero and the lift is negligible because of the cross-sectional symmetry if  $\alpha \approx 0$ . The unsteady torsional moment  $M_{oz}$  (2) is a function of reduced frequency  $k = \omega b/U$  (with  $\omega$  angular motion frequency), and depends on the position along the vertical axis z. The quantity  $k_{\alpha} = \omega_{\alpha}b/U$  denotes the reduced frequency of the apparatus, U is the mean wind speed parallel to the x axis,  $\rho$  is the air density, and  $C(k,z) = F(k,z) + \hat{i}G(k,z)$  is the complex Theodorsen function [23], with  $\hat{i}$  being the imaginary unit. Contrary to standard aeroelastic loads theory [22], the Theodorsen function depends on the coordinate z that simulates variability along the z axis. The derivatives  $\alpha''$  and  $\alpha'$  are computed with respect to the dimensionless time  $s = tU/b = \tau/k_{\alpha}$ ; three-dimensional static load effect is accounted through the function  $\eta_{3D} \approx AR/(AR+2)$ , with AR being the aspect ratio of the blade airfoil  $(AR = \ell/b)$ . In Eq. (2) the variability of the mean wind speed along the vertical direction is not considered, since the aspect ratio AR is assumed to be small.

If the damping ratio  $\zeta_{\alpha}$  is very small, it can be neglected compared to equivalent aeroelastic effects. Substitution of a simple harmonic solution in Eq. (1) at incipient flutter leads to an algebraic homogeneous equation that must be solved for the simultaneous vanishing of its real and imaginary parts. After manipulation, the following algebraic equations are found (with  $\eta = z/\ell$ ):

$$\gamma^2 = 1 + \varepsilon_0 \ell \eta_{3D} \left\{ \int_0^1 \left[ (0.125 + a^2) + \frac{1}{k^2} (2a + 1) F(k, \eta) + \frac{1}{k} (2a^2 - 0.5) G(k, \eta) \right] d\eta \right\}$$
 (3)

$$\int_0^1 \left[ -G(k,\eta)(2a+1) + k(0.5-a) + kF(k,\eta)(2a^2 - 0.5) \right] d\eta = 0$$
 (4)

In Eq. (3),  $\gamma = \omega_{\alpha}/\omega$  is the frequency ratio between the angular frequency of the system  $(\omega_{\alpha})$  and the frequency of the flutter harmonic motion  $(\omega)$ . The coefficient  $\varepsilon_0 = \varepsilon/\ell = \pi \rho b^4 (I_{o\alpha})^{-1}$  is a dimensionless inertia parameter per unit length and  $\eta = z/\ell$  is the dimensionless coordinate in the vertical direction. The frequency at incipient flutter  $k = k^*$  can be found by solving numerically Eq. (4) first; then the frequency ratio at incipient flutter  $\gamma^*$  is computed by solving Eq. (3). Finally, the dimensional, critical flutter wind speed [m/s] can be found as:

$$U^* = \frac{\omega_{\alpha} b}{k^* \gamma^*} \tag{5}$$

## 3. Random variation of aeroelastic loads: modeling & results

The main difficulty in solving flutter problems is the definition of suitable aeroelastic loads or expressions. This issue may lead to modelling simplifications (for thin airfoils [23]) and random errors. In previous work [20] the Theodorsen functions F(k) and G(k) were considered as ideal, independent of z (or  $\eta$ ) and deterministic quantities. If flutter derivatives of the blade cross-sections are measured experimentally, non-negligible variations can be observed; variability can be attributed to experimental laboratory errors. As resulted from wind tunnel tests performed by Li et al. [24], important variability in the flutter derivatives can be noted, especially at higher reduced velocities. Therefore, random variability in the Theodorsen function must be considered when dealing with flutter of blade airfoils. Furthermore, the Theodorsen theory and C(k) function are unable to fully capture the unsteady flow features of wind turbine blade cross-sections [24].

Specifically, this section investigates the influence of stochastic perturbations in the aeroelastic loads effects on the critical frequency and wind speed at flutter. Randomness is introduced in F(k) and G(k). The most promising probability distribution model that describes this variability is the Gaussian one [24]. Monte Carlo simulations are performed to examine this effect.

doi:10.1088/1742-6596/2647/11/112009

Previous studies [20] have identified the leading-edge position (a=-1) of the rotation axis as the optimal configuration for the system; this pivot position minimizes the critical flutter wind speed and ensures wide-range operational conditions. Moreover, a small value of the dimensionless inertia parameter  $\varepsilon = \varepsilon_0 \ell$  has been recommended [20] in the range  $0 < \varepsilon < 1E-3$ . Therefore, a leading-edge configuration with  $\varepsilon = 0.5E-3$  is considered in the subsequent simulations. Eqs. (3)-(4) are iteratively solved by replacing both deterministic functions G(k) and F(k) with two Gaussian variables with mean value equal to the theoretical function at each frequency k and a specified coefficient of variation  $\cos (0.5)$ . The aerodynamic moment  $\delta (0.5)$  is assumed to be uniform along the vertical axis of the blade, independent of  $\delta (0.5)$  or  $\delta (0.5)$  is small. Therefore,  $\delta (0.5)$  and  $\delta (0.5)$  are functions of the reduced frequency  $\delta (0.5)$  and  $\delta (0.5)$  are perfectly correlated with  $\delta (0.5)$  in the first case the Gaussian variables of  $\delta (0.5)$  and  $\delta (0.5)$  are perfectly correlated with cover  $\delta (0.5)$  (i.e., they differ only in their mean values). In the second case the variables are assumed independent with the same  $\delta (0.5)$  in the last two cases the functions  $\delta (0.5)$  and  $\delta (0.5)$  are in turn assumed deterministic. The four cases are described in Table 1, noting that when the correlation coefficient  $\delta (0.5)$  the distributions are fully correlated.

Table 1: Coefficient of variation (cov) and correlation coefficient ( $\rho$ ) of F(k) and G(k) Gaussian random variables.

Case	cov(F) [%]	cov(G) [%]	ρ [-]
1	5	5	1
2	5	5	0
3	5	0	0
4	0	5	0

As an example, Fig. 2 illustrates the empirical histograms of F(k) and G(k), the output distributions of reduced frequency at flutter  $k^*$  and dimensionless critical wind speed  $[\tilde{U}^* = (k^*\gamma^*)^{-1}]$  for the simulation case 2. A sample population equal to 4000 is used to generate the histograms.

The dashed vertical lines are the results when the F(k) and G(k) functions are deterministic  $(k^* = 0.040, \tilde{U}^* = 29.37)$ . The distributions, obtained for other simulation cases, are not reported for the sake of brevity but they exhibit similar patterns. The resulting output histograms are no longer Gaussian and can be approximated by skewed histograms; therefore, the reference estimates of the critical flutter output parameters are computed as the most probable value of the empirical distributions (mode). The coefficient of variation of the reduced frequency at flutter and the critical wind speed, along with the mode of the samples, are reported in Table 2 for the four cases. The percentages of the relative differences  $\hat{\delta}$  between the mode estimates and the values obtained with deterministic aeroelastic forces, are also indicated.

Table 2 clearly shows that the uncertainties in the aeroelastic coefficients are reflected and amplified in the estimates of the critical flutter parameters. The variable that is most affected by the random errors is the critical velocity, as it accounts for both the uncertainties in the frequency ratio  $(\gamma^*)$  and critical reduced frequency  $(k^*)$ . The distributions of the critical wind speed are always more dispersed than the distribution of  $k^*$  and, especially in cases 2 and 4, the output coefficient of variation is one order of magnitude greater than the one introduced in the aeroelastic input variables (cov = 5%). Small errors in the estimation of the functions F(k) and G(k) may lead to large variability in the estimates of the critical flutter velocity. Flutter

doi:10.1088/1742-6596/2647/11/112009

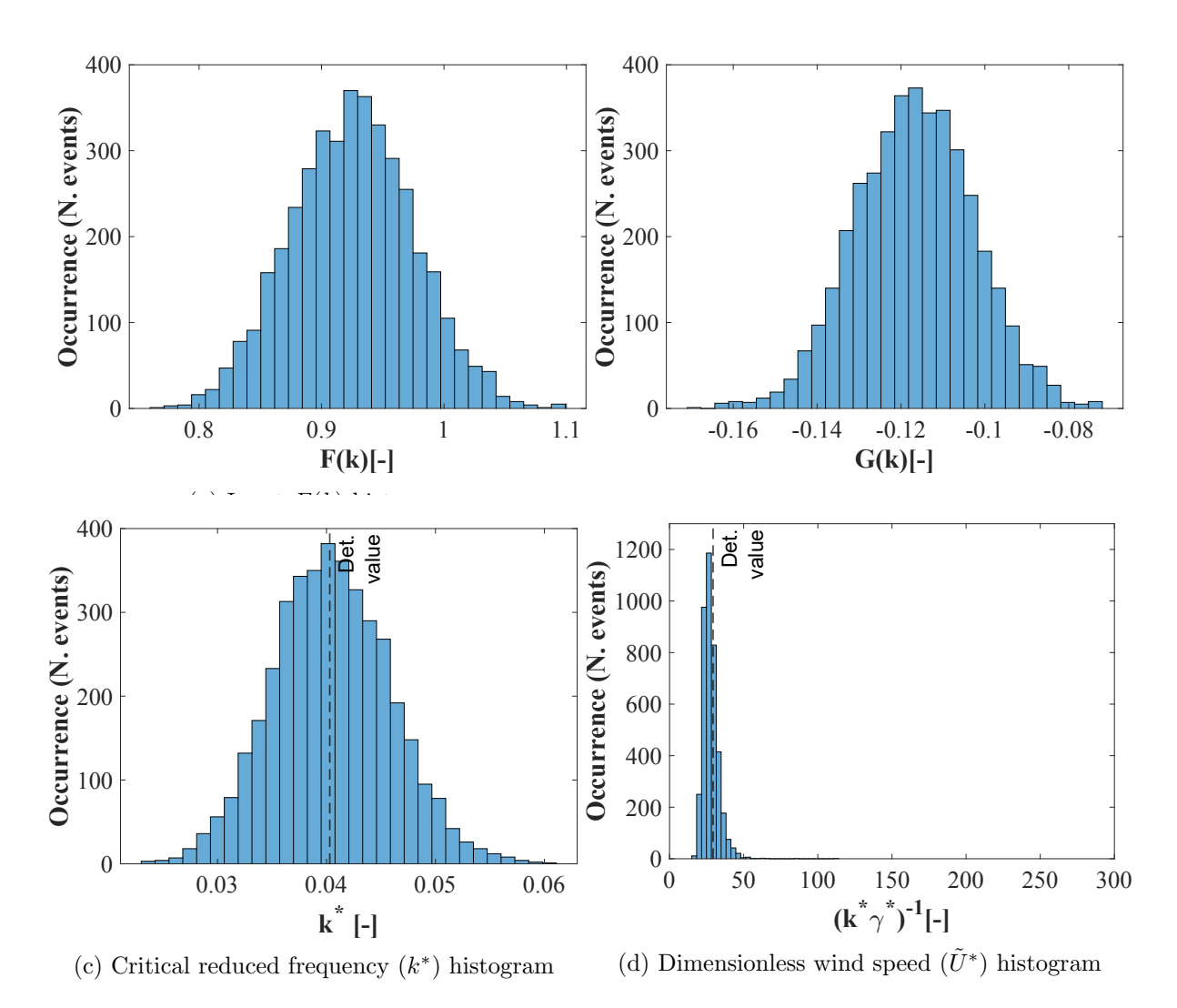


Figure 2: Example of Monte Carlo simulations for the case 2.

Table 2: Mode and coefficient of variation of  $k^*$  and  $\tilde{U}^*$ .

Case	$mode(k^*)$	$\hat{\delta}_{k^*}$	$cov(k^*)$	$\operatorname{mode}\left(\tilde{U}^{*}\right)$	$\hat{\delta}_{ ilde{U}^*}$	$\operatorname{cov}\left(\tilde{U}^{*}\right)$
	[-]	[%]	[%]	[-]	[%]	[%]
1	0.038	11.63	6.4	21.96	25.22	7.42
2	0.036	16.27	13.31	16.86	42.59	19.14
3	0.040	0	6.0	21.15	28.0	7.9
4	0.040	0	12.0	17.67	39.8	16.26

may not even occur if the uncertainties in F(k) and G(k) are simultaneously considered. In case 2 for example, two sample populations with 4000 (equal to 0.05%) repeated simulations do not provide a solution to the flutter condition as there is no root of Eq. (4). The occurrence of no-flutter condition increases to 4.4% samples when cov = 10% is used to simulate the random

distribution of F(k) and G(k). When comparing the four cases presented above, it is worth noting that the aeroelastic coefficient that mostly affects the output uncertainties is G(k), as the coefficients of variation of both  $k^*$  and  $\tilde{U}^*$  are much larger in case 4 than in case 3. This remark is consistent with the idea that torsional flutter is governed by equivalent aeroelastic damping effects, and the G(k) function constitutes the imaginary part of the aeroelastic load, i.e., in phase with the torsional angular velocity. The case with independent random errors of G(k) and F(k) (case 2) is the "worst" scenario, as the predicted flutter speed and frequency are less accurate (i.e., the standard deviation of the output distribution is larger) than in the case of perfectly correlated errors (case 1).

# 4. Incoming turbulence effects: modeling & results

The effect of the incoming turbulence on the frequency at incipient flutter and the critical wind speed is investigated in this section. This problem has been already addressed by Scanlan [25] for long span bridges, who developed an analytical model of the aeroelastic deck load that accounted for the incoming turbulence by considering a spanwise diminution of coherence in the aeroelastic coefficients (flutter derivatives), similar to F(k,z) and G(k,z). Consequently, the dynamic response of the considered apparatus under turbulent flow is studied by considering a loss of coherence of the functions F(k,z) and G(k,z) along the vertical (or longitudinal) axis of the apparatus (z or  $\eta = z/\ell$ ). More specifically, a standard exponential reduction in the coherence of the aeroelastic coefficients is postulated. This is, for F(k,z):

$$F(k,\xi)F(k,\eta) = F(k)^{2} e^{-\frac{k}{2\pi}c\frac{l}{b}|\xi-\eta|}$$
(6)

with  $0 \le \xi \le 1$  and  $0 \le \eta \le 1$  being two dimensionless coordinates, and  $c \ge 0$  a dimensionless coherence parameter. If turbulence effects are neglected  $c \to 0$  and the solution without turbulence is recovered. Experimental evaluations of c suggest that typical values of the coherence parameter are between 5 and 15 [26].

The same format as in Eq. (6) is also used for the product of the  $G(k, \eta)$  function by itself and the cross product between the functions  $G(k, \eta)$  and  $F(k, \eta)$ . Multiplication of Eq. (4) and Eq. (3) by themselves leads to the following equations:

$$\psi^2 = \frac{1}{k^4} (2a+1)^2 F(k)^2 \hat{I} + \frac{1}{k^2} (2a^2 - 0.5) G(k)^2 \hat{I} + \frac{1}{k^3} (2a+1) (2a^2 - 0.5) F(k) G(k) \hat{I}$$
 (7)

$$(2a+1)^2G(k)^2\hat{I} + k^2(2a^2-0.5)^2F(k)^2\hat{I} - 2(2a+1)k(2a^2-0.5)G(k)F(k)\hat{I} - k^2(0.5-a)^2 = 0 \ \ (8)^2G(k)^2\hat{I} + k^2(2a^2-0.5)^2F(k)^2\hat{I} - 2(2a+1)k(2a^2-0.5)G(k)F(k)\hat{I} - k^2(0.5-a)^2 = 0 \ \ (8)^2G(k)^2\hat{I} + k^2(2a^2-0.5)^2F(k)^2\hat{I} - 2(2a+1)k(2a^2-0.5)G(k)F(k)\hat{I} - k^2(0.5-a)^2 = 0 \ \ (8)^2G(k)^2\hat{I} + k^2(2a^2-0.5)^2F(k)^2\hat{I} - 2(2a+1)k(2a^2-0.5)G(k)F(k)\hat{I} - k^2(0.5-a)^2 = 0 \ \ (8)^2G(k)$$

where  $\psi = \left[\frac{\gamma^2 - 1}{\epsilon \eta_{3D}} - (0.125 + a^2)\right]$  and  $\hat{I}$  is the integral of the co-coherence function, whose closed-form expression is reported in Eq. (9) below, with  $\hat{k} = \frac{k}{2\pi} c \frac{\ell}{b}$ .

$$\hat{I}(k,c,AR) = \int_0^1 \int_0^1 e^{-\frac{k}{2\pi}c\frac{l}{b}|\xi-\eta|} d\xi d\eta = \frac{2}{\hat{k}^2} (-1 + e^{-\hat{k}} + \hat{k})$$
(9)

As the integral  $\hat{I}$  depends on  $\ell/b$ , the turbulence effects introduce the dependency of the reduced frequency at flutter on the aspect ratio. On the contrary, the previous Eq. (4) does not depend on the aspect ratio, inertia and other physical quantities. The integral  $\hat{I}$  is plotted in Fig. 3 as a function of the reduced frequency k for two different values of the aspect ratio AR and for c = 10. The proposed closed form solution [Eq. (9)] is valid as long as  $\hat{k} \neq 0$ . As k (and  $\hat{k}$ ) reduces, the value of  $\hat{I}$  tends to 1.

doi:10.1088/1742-6596/2647/11/112009

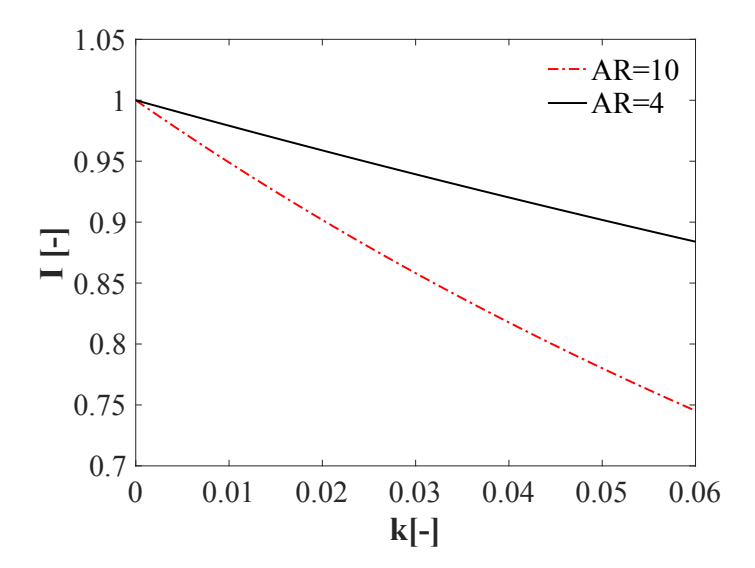


Figure 3: Integral  $\hat{I}$  as a function of the reduced frequency for c=10 and AR=4,10.

The imaginary part of the governing homogeneous equation (i.e., the left hand side of Eq. (8)) is represented in Fig. 4 for different values of the coherence parameter c when AR = 10. As the coherence of the dynamic coefficients increases, the function becomes flatter and the reduced frequency at flutter increases.

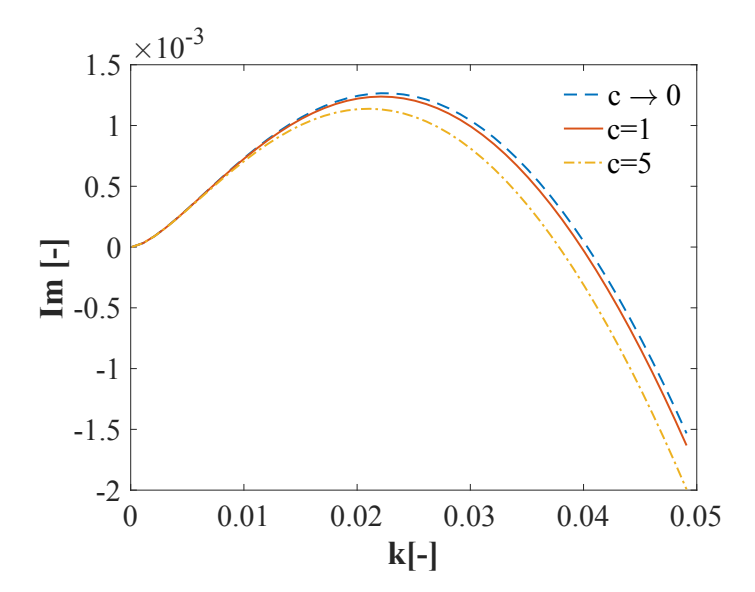


Figure 4: Imaginary part of the homogeneous governing equation (AR = 10).

Equation (8) can be first solved to get the critical value of k; then Equation (7) is used to compute  $\psi^*$  and the critical wind speed under turbulence effects from  $\gamma_u^*$ :

$$\gamma_u^{2*} = \left[ \mp \psi^* + (0.125 + a^2) \right] \varepsilon \eta_{3D} + 1 \tag{10}$$

Equation (10) provides two distinct solutions for the critical wind speed depending on the sign of the variable  $\psi^*$ . The critical wind speed at flutter  $k_u^*$  and the two sets of critical wind speed  $\tilde{U}_u^{*\pm}$  are reported in Tab. 3 for different values of the coherence parameter (c) and aspect

ratio (AR). The solution without turbulence effect  $\tilde{U}^*$  is recovered when negative values of  $\psi^*$  are used in Eq. (10). Fig. 5 illustrates the evolution of the reduced frequency at flutter and critical wind speed  $\tilde{U}_u^{*-}$  as a function of the coherence parameter c. When the turbulence effect increases the reduced frequency at flutter decreases and the critical wind speed increases. The efficiency of the apparatus is therefore expected to reduce as the turbulence effect becomes more important. When the  $\ell$  dimension of the harvester in the vertical direction reduces and AR decreases, the system is less sensitive to the incoming turbulence.

Table 3: Reduced frequency  $k^*$  and critical wind speed  $\tilde{U}_n^*$  at varying coherence c.

			$c \to 0$	c = 1	c = 5	c = 10
$AR \to \infty$	$(\tilde{U}^* = 29.37)$	$\begin{array}{c} k_u^* \\ \tilde{U}_u^{*-} \\ \tilde{U}_u^{*+} \end{array}$	0.0403 29.22 21.87	0.0357 34.17 82.39	0.0261 54.97 91.92	0.0206 94.47 95.73
AR = 10	$(\tilde{U}^* = 28.40)$	$\begin{array}{c} k_u^* \\ \tilde{U}_u^{*-} \\ \tilde{U}_u^{*+} \end{array}$	0.0403 28.40 22.26	0.0398 28.87 22.53	0.0378 30.71 23.55	0.0357 32.97 24.73
AR = 4	$(\tilde{U}^* = 27.55)$	$\begin{array}{c} k_u^* \\ \tilde{U}_u^{*-} \\ \tilde{U}_u^{*+} \end{array}$	0.0403 27.57 22.72	0.0401 27.73 22.82	0.0393 28.42 23.26	0.0383 29.27 23.79

[Note: critical wind speed without turbulence effect  $\tilde{U}^*$  is shown within parentheses.]

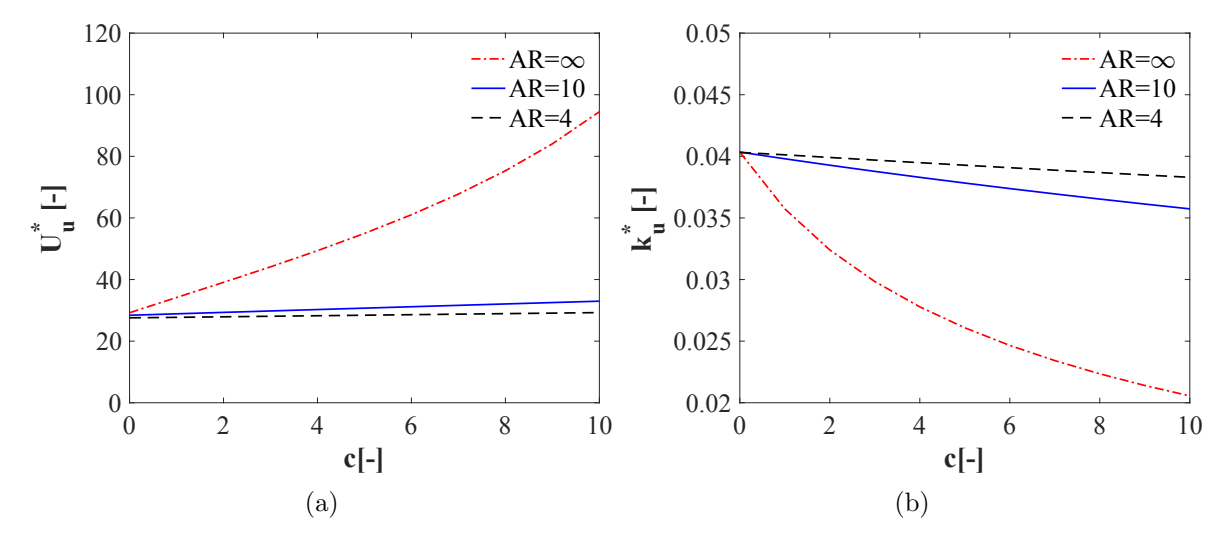


Figure 5: Turbulence effect as a function of the dimensionless coherence parameter c: (a) critical wind speed, (b) reduced frequency at flutter.

### 5. Conclusions

In this paper, stochastic simulations are performed to describe the influence of turbulence and random error in modelling the aeroelastic loads that describe the behavior of a wind energy

doi:10.1088/1742-6596/2647/11/112009

harvester. Random variability is first introduced in the Theodorsen function; results show that the critical wind speed is strongly affected by the introduced error. The aerodynamic coefficient that mostly affect the uncertainty in the prediction of incipient flutter condition is G(k), as it constitutes the (imaginary) part of the load in phase with the angular velocity. The incoming turbulence effect is separately investigated in the last section of the paper, where the approach proposed by Scanlan [25] for bridges is adapted to the case study. When the turbulence is taken into account, the efficiency of the apparatus reduces as the critical wind speed increases. Finally, the sensitivity to turbulence effects is enhanced as the aspect ratio  $AR = \ell/b$  increases.

# Acknowledgments

This work was supported in part by the National Science Foundation (NSF) of the United States of America, Award CMMI-2020063. Any opinions, findings and conclusions or recommendations are those of the authors and do not necessarily reflect the views of the NSF.

#### References

- [1] Priya S and Inman D 2009 Energy Harvesting Technologies (New York, NY: Springer)
- [2] Caracoglia L 2010 J. Wind Eng. Ind. Aerodyn. 98 679–686
- [3] Duncan W J 1945 Aircr. Eng. Aerosp. Technol. 17 16–20
- [4] McKinney W and DeLaurier J 1981 J. Energy 109-115
- [5] Young J, Lai J C and Platzer M F 2014 Prog. Aerosp. Sci. 67 2–28
- [6] Ahmadi G 1979 Wind. Enq. 3 207–215
- [7] Ahmadi G 1978 Energy Conversion 18 115–120
- [8] Tang L, Paidoussis M and Jin J 2009 J. Sound Vib. 326 263-276
- [9] Matsumoto M, Mizuno K, Okubo K and Ito Y 2006 American Society of Mechanical Engineers, Pressure Vessels & Piping Division Conference (PVP) pp 277–286
- [10] Matsumoto M 2013 J. Wind Eng. Ind. Aerodyn. 122 10–20
- [11] Kinsey T and Dumas G 2008 AIAA J. 46 1318–1330
- [12] Shimizu E, Isogai K and Obayashi S 2008 J. Fluids Eng. Trans. ASME 130 0211041-0211048
- [13] Isogai M, Yamasaki K, Matsubara M and Asaoka T 2003 Int. Forum Aeroelasticity Struct. Dyn.
- [14] Kinsey T, Dumas G, Lalande G, Ruel J, Méhut A, Viarouge P, Lemay J and Jean Y 2011 Renew. Energy 36 1710–1718
- [15] Jones K, Davids S and Platzer M 1999 3rd ASME/JSME Joint Fluids Eng. Conf. San Francisco CA, USA pp 18–23
- [16] Pigolotti L, Mannini C, Bartoli G and Thiele K 2017 J. Sound Vib. 404 116–140
- [17] Hoke C M, Young J, Lai J C, Karakas F, Zaloglu B and Fenercioglu I 2017 Procedia Eng. 199 3450-3455
- [18] D'Adamo J, Collaud M, Sosa R and Godoy-Diana R 2022 Bioinspiration and Biomimetics 17 ISSN 17483190 (Preprint 2206.01647)
- [19] Duarte L, Dellinger N, Dellinger G, Ghenaim A and Terfous A 2021 Renew. Energy 171 1436-1444
- [20] Caracoglia L 2017 Procedia Eng. 199 3434–3439
- [21] Kwon S D, Park J and Law K 2013 Smart Mater. Struct. 22 055007
- [22] Bisplinghoff R L, Ashley H and Halfman R L 1955 Aeroelasticity (Mineola, NY, USA: Dover Publications Inc.)
- [23] Theodorsen T 1935 General theory of aerodynamic instability and the mechanism of flutter Technical Report (TR) 496 National Advisory Committee for Aeronautics
- [24] Li S, Caracoglia L and Møller-Madsen J 2023 J. Fluids Struct. 118 103843
- [25] Scanlan R H 1997 J. Struct. Eng. **123** 232–236
- [26] Solari G 1987 J. Struct. Eng. 113 (7) 1550–1569